Dressed-state control of effective dipolar interaction between strongly-coupled solid-state spins

Junghyun Lee,[1,2] Mamiko Tatsuta,[3] Andrew Xu,[1,*] Erik Bauch,[4] Mark J. H. Ku,[5,4,†] and Ronald. L. Walsworth[5,4,6,‡]

[1]*Department of Physics, Massachusetts Institute of Technology, Cambridge, MA 02139, USA*
[2]*Korea Institute of Science and Technology, Center for Quantum Information, Seoul 02792, Republic of Korea*
[3]*Research Center for Emerging Computing Technologies, National institute of Advanced Industrial Science and Technology (AIST), Central2, 1-1-1 Umezono, Tsukuba, Ibaraki 305-8568, Japan*
[4]*Department of Physics, Harvard University, Cambridge, MA 02138, USA*
[5]*Harvard-Smithsonian Center for Astrophysics, Cambridge, MA 02138, USA*
[6]*Center for Brain Science, Harvard University, Cambridge, MA 02138, USA*

(Dated: March 16, 2022)

Strong interactions between spins in many-body solid-state quantum system is a crucial resource for exploring and applying non-classical states. In particular, electronic spins associated with defects in diamond system are a leading platform for the study of collective quantum phenomena and for quantum technology applications. While such solid-state quantum defect systems have the advantage of scalability and operation under ambient conditions, they face the key challenge of controlling interactions between the defects spins, since the defects are spatially fixed inside the host lattice with relative positions that cannot be well controlled during fabrication. In this work, we present a dressed-state approach to control the effective dipolar coupling between solid-state spins; and then demonstrate this scheme experimentally using two strongly-coupled nitrogen vacancy (NV) centers in diamond. Including Rabi driving terms between the $m_s = 0$ and ±1 states in the NV spin Hamiltonian allows us to turn on and off or tune the effective dipolar coupling between two NV spins. Through Ramsey spectroscopy, we detect the change of the effective dipolar field generated by the control NV spin prepared in different dressed states. To observe the change of interaction dynamics, we then deploy spin-lock-based polarization transfer measurements via a Hartmann-Hahn matching condition between two NV spins in different dressed states. We perform simulations that indicate the promise for this robust scheme to control the distribution of interaction strengths in strongly-interacting spin systems, including interaction strength homogenization in a spin ensemble, which can be a valuable tool for studying non-equilibrium quantum phases and generating high fidelity multi-spin correlated states for quantum-enhanced sensing.

I. INTRODUCTION

Understanding and engineering of strongly-coupled solid-state quantum spin systems is a key challenge for quantum technology. Such systems could be utilized to observe and generate collective quantum behaviour, leading to highly sought-after applications ranging from quantum simulation of non-equilibrium phases [1–3] to quantum enhanced sensing applications beyond the classical limit [4–6]. In particular, recent work using nitrogen-vacancy (NV) centers in diamond have addressed challenging problems such as the observation of critical thermalization in a three dimensional ensemble [1], and a Discrete Time Crystal (DTC) state subject to a periodic drive in a disordered spin ensemble [2]. Realization of a strongly interacting, many-spin system was possible through the fabrication of dense NV ensembles in diamond samples with both large nitrogen density ([N]) and high [N] to [NV] conversion yield [1, 7]. In this regime, NV-NV dipolar couplings are the dominant spin interactions [1, 8], with robust control possible for an ensemble of NV spins at ambient temperature.

To build on this progress and realize the aforementioned applications, it is crucial to have deterministic control of interactions between the strongly-coupled solid-state spins. To date, such control has not been possible in a scalable manner, due to variation in spin-spin separation from the stochastic process by which quantum defects are fabricated in the host solid [9]. Nanoscale spatial precision of defect formation has recently been demonstrated [10, 11], yet the generation of ensembles of solid-state spins still largely depends on the stochastic methods of ion implantation [12, 13] and chemical vapor deposition [14], leading to a wide variation ($>10\times$) in the distribution of spin-spin interactions. The lack of control over such spin-spin interactions limits the utility of solid-state spin systems for many-body simulations and the generation of multipartite entanglement for quantum-enhanced sensing [15].

In this work, we present a method to continuously modulate the dipolar coupling between strongly-coupled spin-1 qutrits through the manipulation of dressed states.

* Now at Pritzker School of Molecular Engineering, University of Chicago, Chicago, IL 60637, USA
† Now at Department of Physics and Astronomy, University of Delaware
‡ walsworth@umd.edu; Now at Department of Physics, University of Maryland

We use a strongly-coupled pair of NV centers in diamond as a testbed to demonstrate the approach. The negatively charged NV center is effectively a two electron system [16], forming an S = 1 spin qutrit. The present study builds on past work where pairs of strongly interacting electronic spins in diamond were utilized to study coherent manipulation of an electronic dark spin [17], as well as generation of a room temperature entangled state [18]. Here, we employ two Rabi driving fields to induce an oscillating NV spin population between both the $m_s = 0$ and -1 level and the $m_s = 0$ and $+1$ level, thereby generating a spin qutrit dressed state. With such a doubly dressed state, an effective dipolar coupling between the two NV spins (labelled NV_A and NV_B) can be modulated by careful apportion of the relative Rabi driving field magnitudes. This dressed state scheme provides a robust tuning knob for an NV ensemble spin system. In future work, this technique may enable quantum-enhanced sensing, and allow engineering of the NV-NV coupling dynamics or local disorder amplitude to study transitions of non-equilibrium phases [1, 2].

Generating dressed states in an interacting spin-1/2 system via introducing driving fields to decouple dipolar interactions (also referred to as motional narrowing) has been extensively studied in diverse systems such as NMR [19, 20] and superconducting qubits [21]. For spin defects in diamond, a single Rabi driving field was applied to spin-1/2 nitrogen electronic spins (P1s) to suppress the overall dipolar field noise on NV spins [22, 23]. However, more complicated dynamics can arise for strongly-coupled spin-1 qutrits [24], such as for dense ensembles of NV electronic spins, thereby requiring further analysis and experimental investigation, as presented here.

To begin, we consider a simple 2 qutrit spin Hamiltonian with driving terms. With the spin flip-flop terms neglected for the dipolar interaction between the NV electronic spins [1], the total time-dependent Hamiltonian of the system with driving fields is simplified as

$$H(t) = \sum_{i\in(A,B)} \left(D(S_i^z)^2 + \gamma B_i S_i^z\right) + \sum_{i\in(1,2)} \Omega_{A,i}\cos(\omega_{A,i}t)S_A^x + \sum_{i\in(1,2)} \Omega_{B,i}\cos(\omega_{B,i}t)S_B^x + \nu S_A^z S_B^z \tag{1}$$

where D denotes the zero-field splitting, γB_i is the bias magnetic field Zeeman splitting with gyromagnetic ratio γ, ν parameterizes the magnetic dipolar coupling between the two NV spins $\vec{S}_A$ and $\vec{S}_B$, and $\Omega_{(A,B),1}$, $\Omega_{(A,B),2}$ are the Rabi frequencies of external microwave fields that drive the $|m_s = 0\rangle \leftrightarrow |m_s = -1\rangle$ and $|m_s = 0\rangle \leftrightarrow |m_s = +1\rangle$ transitions for NV_A and NV_B, respectively, at near-resonant frequencies $\omega_{A,B}$. In our experiment, we apply Rabi driving to one NV spin (NV_B) while detecting the resulting effect with the second, sensing spin NV_A. By letting $\Omega_{A,(1,2)} = 0$ and $\Omega_{B,(1,2)} = \Omega_{1,2}$, the overall Hamiltonian can be diagonalized in the $S_A^z \otimes S_B^z$ basis in a doubly rotating frame with the rotating wave approximation. The effective dipolar coupling term can then be analytically solved, under the condition of $\nu \ll \Omega_{1,2}$, yielding:

$$\nu_{eff} \approx \frac{1}{2}\frac{(\Omega_1^2 - \Omega_2^2)}{(\Omega_1^2 + \Omega_2^2)}\nu \tag{2}$$

For a detailed discussion on the calculation, see the supplementary material Appendix C. Eq. (2) indicates that by tuning $\Omega_{1,2}$, we can continuously vary the effective dipolar coupling strength between -$\nu/2$ and +$\nu/2$. Eq. (2) is a generalized formula that provides different driving conditions; e.g., $\Omega_1 = \Omega_2$, $\nu_{eff} = 0$; $\Omega_2 = 0$, $\nu_{eff} = \nu/2$; $\Omega_1 = 0$, $\nu_{eff} = -\nu/2$.

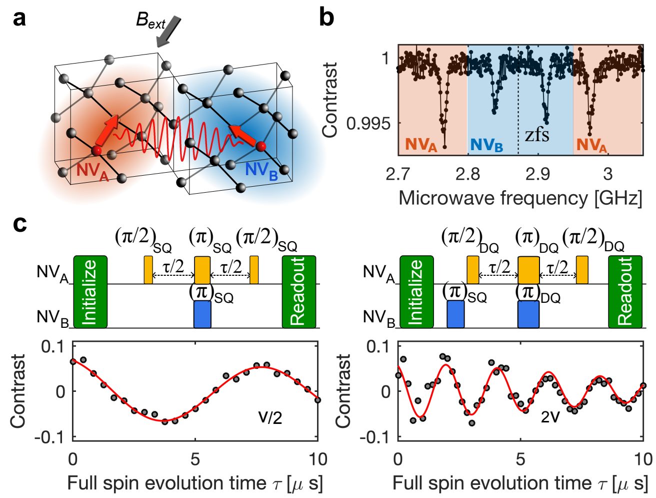

FIG. 1. Characterization of two NV qutrit spin system. (a) Schematic of two strongly-coupled NVs inside the diamond lattice, separated by ¡ 10 nm. External bias magnetic field B_{ext} is aligned with the quantization axis of the sensor spin NV_A (red); the control spin NV_B (blue) has a different quantization axis. (b) Optically detected magnetic resonance (ODMR) measurement of NV pair system. With different Zeeman splittings due to different B_{ext} field projections on each NV quantization axis, NV_A and NV_B are resolved in the frequency domain. (c) Double electron-electron resonance (DEER) measurement pulse sequences and measurement results. NV_A is used as a sensing spin in both the single quantum (SQ, left) and double quantum (DQ, right) basis. NV_B is used as a control spin, π flipped from $m_s = 0$ to $m_s = +1$ (left) and double π flipped from $m_s = -1$ to $m_s = +1$ (right). From the resulting modulation frequencies of the SQ and DQ DEER measurements, we extract the NV_A-NV_B dipolar coupling strength of $\nu = 0.250 \pm 0.015$ MHz.

II. RESULTS

To realize an isolated system of two strongly-coupled NV qutrit spins (with $\nu > \Delta_{bath} \approx \frac{1}{T_2^*}$, where Δ_{bath} is the effective coupling strength between the NV and bath spins), we use a molecular implantation technique [17, 25]. More details on the diamond sample is discussed in the supplementary material Appendix B. We first deploy a double electron-electron resonance (DEER) measurement protocol to measure the intrinsic coupling strength between two neighboring and strongly-coupled NV spins. Due to DEER's spin echo based pulse scheme, the NV_A sensing spin accumulates net phase only to the repeated inversion of the NV_B control spin, filtering out other possible magnetic signal sources at frequencies lower than the NV_B spin modulation. To directly observe the change of NV-NV interaction dynamics under different dressed states, NV-NV polarization transfer via a spin-lock pulse sequence is used. To enable the polarization transfer measurement, we perform Ramsey spectroscopy on NV_A for different polarizations of NV_B: this measurement characterizes the effective NV-NV dipolar field under different dressed states. Note that the roles of NV_A and NV_B can be interchanged in all the results presented here.

A. DEER measurements

We use a DEER pulse sequence to measure the coupling strength between two strongly interacting NV spins. We select neighboring NVs with different quantization axes (Fig. 1a), which allows us to distinguish the two NV spins in the ODMR frequency domain (Fig. 1b), thereby allowing individual NV spin control. The DEER technique measures the dynamic phase accumulated by the sensor spin (NV_A) due to the dipolar magnetic field generated by the control spin (NV_B). First, we performed a DEER measurement in the single quantum (SQ) basis of $|0\rangle$ and $|+1\rangle$ states. The NV_A-NV_B interaction is given by an Ising term with coupling strength ν (Equation (1)). The accumulated phase is projected back to $|0\rangle$ for NV_A via a probability measurement $P_{SQ} \propto \cos(\nu\tau/2)$. Meanwhile, under the double quantum (DQ) basis of $|B\rangle = \frac{|+1\rangle+|-1\rangle}{\sqrt{2}}$ and $|D\rangle = \frac{|+1\rangle-|-1\rangle}{\sqrt{2}}$ for NV_A, and $|-1\rangle$, $|+1\rangle$ states for NV_B, the accumulated phase projected back to $|0\rangle$ for NV_A is given by $P_{DQ} \propto \cos(2\nu\tau)$. In the SQ basis of sensor spin NV_A with the control spin NV_B flipped to $|+1\rangle$ after being initialized to $|0\rangle$, we measure a DEER signal oscillation of $\nu/2 = 0.125 \pm 0.01$ MHz (see Fig. 1c, left). In the DQ basis of sensor spin NV_A with the control spin NV_B flipped to $|+1\rangle$ after being initialized to $|-1\rangle$, we measure a DEER signal oscillation of $2\nu = 0.495 \pm 0.031$ MHz (see Fig. 1c, right). From both these measurements, we extract the NV_A-NV_B dipolar coupling parameter $\nu = 0.250 \pm 0.015$ MHz.

B. Ramsey interferometry

Similar to DEER, Ramsey interferometry also allows the sensing spin NV_A to accumulate dynamic phase due to the static dipolar field produced by the control spin NV_B. Ramsey spectroscopy has been used as a spectroscopic tool to measure the effective coupling strengths between an ensemble of NV spins and a bath of P1 spins [26]. In contrast to DEER, there is no π pulse applied to NV_B during a Ramsey measurement; therefore, the dipolar field is constant for an initially prepared m_s state of NV_B during the phase accumulation of the NV_A spin. For a Ramsey measurement on the NV_A SQ basis of $|0\rangle$ and $|+1\rangle$, when NV_B is prepared in $|0\rangle$, no dynamic phase is accumulated on NV_A due to the zero longitudinal dipolar coupling. However, for NV_B prepared in $|\pm1\rangle$ with non-zero longitudinal dipolar coupling, NV_A exhibits a phase modulation of $\pm\gamma\nu\tau$ during a Ramsey measurement. When a similar Ramsey measurement is performed using the NV_A DQ basis of $|B\rangle$ and $|D\rangle$, the effective magnetic moment of the NV_A spin is doubled and there is thus a twice faster phase accumulation. A fast Fourier transformation (FFT) applied to the Ramsey signal then reveals the phase modulation frequency and hence the dipolar coupling magnitude between the two spins. In our analysis, we focus on one of the three NV hyperfine peaks in the ODMR spectrum. For the Ramsey measurement in the NV_A SQ basis, we find $\pm\nu = 0.26 \pm 0.02$ MHz; see Fig. 2a. In the DQ basis, we determine Ramsey resonance peak shifts of $\pm 2\nu = 0.52 \pm 0.02$ MHz, relative to the peak for the no-interaction case; see Fig. 2b. Uncertainty here is given by the frequency resolution of the FFT. Note that the dipolar coupling strength extracted from SQ and DQ Ramsey spectroscopy agrees with the DEER measurements described above. This coupling strength implies a separation of the two NVs of about 6 nm.

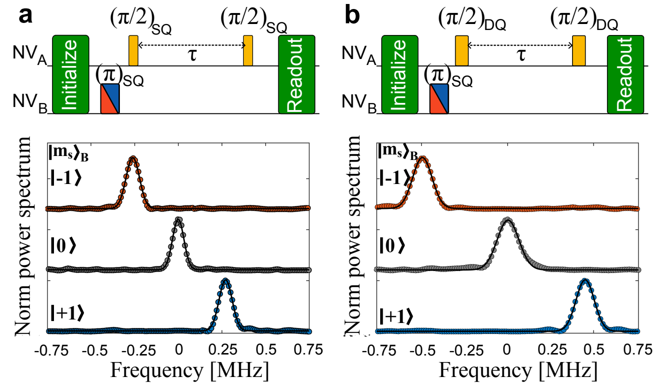

FIG. 2. Ramsey spectroscopy for sensing dipolar coupling strength of two NV qutrit system. (a) Single quantum (SQ) Ramsey spectroscopy pulse sequence varies the evolution time τ of the sensor spin NV_A with the control spin NV_B initialized to $|0\rangle$ (gray), $|+1\rangle$ (blue) and $|-1\rangle$ (red) states. Relative shifts in the peak of the power spectrum of the Ramsey signal as a function of the state of NV_B give the dipolar coupling strength $\nu = 0.26 \pm 0.02$ MHz. (b) Repeat of the same measurement for the double quantum (DQ) basis of NV_A. Due to doubling of the effective magnetic moment of spin NV_A in the DQ basis, twice larger shifts are observed in the Ramsey signal power spectrum, yielding $2\nu = 0.52 \pm 0.02$ MHz.

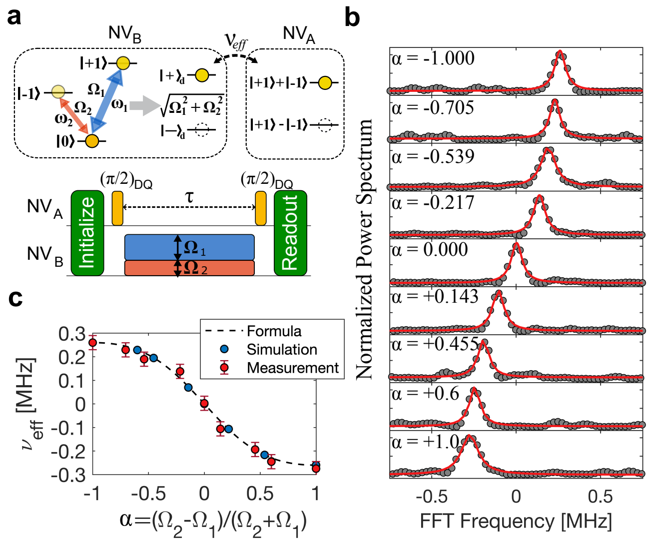

FIG. 3. Tuning effective coupling strength of two NV qutrit system via doubly dressed state. (a) Left inset box shows the ground state energy level of the control spin NV$_B$. Microwave control fields at resonance frequencies ω_1, (between $|0\rangle$ and $|+1\rangle$ states) and ω_2 (between $|0\rangle$ and $|-1\rangle$ states) are driven with Rabi frequencies $\Omega_{1,2}$, which results in an effective two level doubly dressed state $|+\rangle_d, |-\rangle_d$ shown in the right inset box. Below is the pulse sequence for DQ Ramsey spectroscopy on the sensing spin NV$_A$ with NV$_B$ driven by microwave control fields at $\Omega_{1,2}$. (b) Normalized power spectrum of the Ramsey signal for NV$_A$. Gray dots are measurement and red solid lines are Lorentzian fits to the data. Dressed-state control parameter $\alpha = \frac{(\Omega_1 - \Omega_2)}{(\Omega_1 + \Omega_2)}$. For NV$_B$ driven on only a single transition, i.e., for $\alpha = \pm 1$, a modulation peak is observed at the bare dipolar coupling strength between the two NVs ($\pm\nu$) because phase is accumulated in NV$_A$'s DQ basis. For NV$_B$ driven on both transitions with the same Rabi frequency, i.e., for $\alpha = 0$, a peak appears at FFT frequency = 0. As α is swept from -1 to +1 with $\Omega_{1,2} > 2$ MHz $> \nu$, the modulation peak continuously shifts from $\nu_{eff} = +\nu$ to $\nu_{eff} = -\nu$. (c) Variation of ν_{eff} with dressed-state control parameter α. Red dots are measurements, blue dots are from a numerical simulation, and black dashed line is from Eqn. (2). Simulation is from numerically solving Eqn. (1).

C. Doubly dressed-state control of effective dipolar coupling

We next introduce a driving field on the control spin NV$_B$ to generate a doubly dressed state, as outlined above; and then perform Ramsey detection in the DQ basis of NV$_A$ to sense the resulting interaction dynamics. In a semi-classical spin picture, double driving of the NV$_B$ spin transitions with Rabi frequencies of Ω_1 and Ω_2 transfer population into each spin state $|+1\rangle$ and $|-1\rangle$ proportional to Ω_1^2 and Ω_2^2, respectively. In the fast driving limit of $\nu \ll \Omega_{1,2}$, each population is time-averaged to its half, and the overall net spin population becomes $\frac{1}{2}(\Omega_1^2 - \Omega_2^2)$. Normalizing to the total population $\Omega_1^2 + \Omega_2^2$, we get a time-averaged effective spin number of $m_s^{eff} \approx (\Omega_1^2 - \Omega_2^2)/2(\Omega_1^2 + \Omega_2^2)$; hence, the effective coupling between NV$_A$ and NV$_B$ becomes $\nu_{eff} = m_s^{eff}\nu$, which is in agreement with Eqn. (2). See Fig. 3a. For detection, we monitor the DQ Ramsey power spectrum of one of the NV$_A$ hyperfine peaks in the frequency domain as we change Ω_1 and Ω_2. To satisfy the $\nu \ll \Omega_{1,2}$ condition, all measurements are done with 2 MHz $< \Omega_{1,2}$. We define $\alpha = \frac{(\Omega_1 - \Omega_2)}{(\Omega_1 + \Omega_2)}$ as a control parameter that indicates the degree of relative driving strengths. For example, $\alpha = 0$ for equal Rabi frequencies ($\Omega_1 = \Omega_2$), and $\alpha = +1$ when driving only the single transition $|0\rangle \leftrightarrow |+1\rangle$ ($\Omega_1 \neq 0, \Omega_2 = 0$). As α is swept from -1 to +1, the Ramsey power spectrum peak transitions from $+\nu = +0.26$ MHz to $-\nu =$ -0.26 MHz (Fig. 3b). We confirm that the effective coupling extracted from Eqn. (2) and our numerical simulation, based on Eqn. (1), lie within the measurement error bound (Fig. 3c).

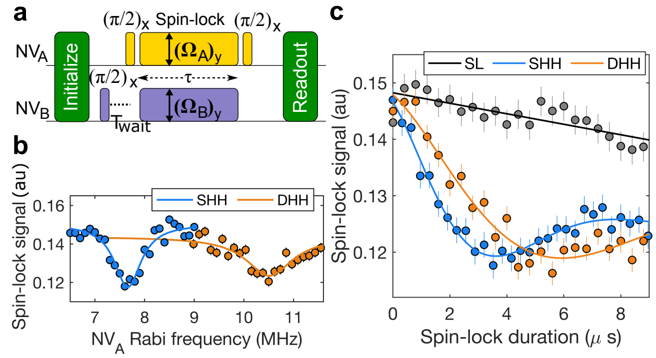

FIG. 4. Spin polarization transfer measurement under singly and doubly dressed state Hartmann-Hahn conditions (SHH and DHH). (a) Polarization transfer pulse sequence. NV$_B$ is first prepared in a $|0\rangle$, $|+1\rangle$ mixed state and then Rabi driven to dressed states, while NV$_A$ is spin-locked along the y-axis. (b) NV$_A$ spin-lock (SL) coherence signal measurement. While sweeping the NV$_A$ Rabi frequency. NV$_B$ is driven to SHH or DHH by controlling the NV$_B$ Rabi frequency $\Omega_{B,(1,2)}$. Once either matching condition is satisfied, $\Omega_A = \sqrt{\Omega_{B,1}^2 + \Omega_{B,2}^2}$, polarization from NV$_A$ is lost, as shown as dips in the SL signal. SHH is when NV$_B$ is singly driven, and DHH is when NV$_B$ is doubly driven. (c) Polarization transfer dynamics measured via the NV$_A$ SL coherence signal over the duration of NV$_A$ spin-lock driving. NV$_A$ Rabi frequencies are fixed at the SHH or DHH matching frequencies with NV$_B$.

D. Polarization transfer in dressed states

To explore the advantage of tuning spin-spin interactions via a doubly dressed state scheme, we employ a dressed state spin polarization measurement [27] with a spin-lock (SL) pulse sequence by varying the $|\pm 1\rangle$ transition Rabi frequencies. Polarization transfer measurements are a useful tool for exploring interaction dynamics within strongly-coupled systems [1]. We choose NV$_A$ as the polarization delivering spin and NV$_B$ as the polarization target spin. NV_B is first initialized and prepared in a fully dephased state in the $|0\rangle, |+1\rangle$ basis by applying a $(\pi/2)_x$ pulse and a wait time $T_{wait} \gg T_2^*$. Then NV_B is driven with single or double transition driving fields by tuning $\Omega_{B,1}(|0\rangle \leftrightarrow |+1\rangle)$ and $\Omega_{B,2}(|0\rangle \leftrightarrow |-1\rangle)$, inducing a change in the effective dipolar coupling between the two NVs in a dressed state picture (Fig. 4a). NV_A is initialized and spin-locked along the y-axis with driving field $\Omega_A(|0\rangle \leftrightarrow |+1\rangle)$. Once the two NVs satisfy either the singly or doubly dressed state Hartmann-Hahn matching conditions (SHH or DHH) [28], only the $\nu_{eff} S_1^z \otimes S_2^z$ term survives in the rotating frame Hamiltonian, inducing transfer of polarization from NV_A to NV_B. For a two-level spin picture, this can be understood as generating resonant energy levels between the two dressed-state spin qubits. The Rabi frequency for each spin corresponds to the energy level splitting in the rotating frame, and by tailoring the Rabi frequency matched dressed states between the two spins, polarization can be exchanged in the double-rotating frame. For an S=1 spin system, a doubly dressed state generates an effective two level system with energy splitting of $\sqrt{\Omega_1^2 + \Omega_2^2}$. Therefore, energy conserving polarization exchange can occur once the singly driven qutrit spin's Rabi frequency matches the other qutrit spin's doubly driven Rabi frequency $\sqrt{\Omega_1^2 + \Omega_2^2}$. For a given NV_B singly or doubly dressed state, the Rabi frequency of NV_A and the SL duration determine the degree and rate of polarization loss(gain) of $NV_A(NV_B)$.

With a fixed spin-lock time τ, Rabi frequency Ω_A is swept to verify the Hartmann-Hahn (HH) matching condition. We apply a $|0\rangle \leftrightarrow |+1\rangle$ single transition driving field to NV_B with Rabi frequency of $\Omega_{B,1} = 7.56$ MHz, and sweep the NV_A Rabi frequency between $|0\rangle \leftrightarrow |+1\rangle$ from Ω_A= 6 to 9 MHz. Here, the SL duration is set to be the inverse of the estimated effective dipolar coupling between the two NVs. A Lorentzian dip is observed in the NV_A SL coherence measurement (Fig. 4b), indicating a loss of polarization from NV_A; the dip is located at Ω_A= 7.66±0.1 MHz, which coincides with the expected SHH matching condition. Next, we apply a double driving field to NV_B, with Rabi frequencies of $\Omega_{B,1}$= 9.59 MHz and $\Omega_{B,2}$= 4.13 MHz, to induce a change in polarization transfer dynamics. Again, the NV_A $|0\rangle \leftrightarrow |+1\rangle$ transition Rabi frequency is swept from Ω_A= 9 to 12 MHz. The DHH matching condition is given by $\Omega_A = \sqrt{\Omega_{B,1}^2 + \Omega_{B,2}^2}$ and the measurement result shows a dip appearing at Ω_A= 10.51 ± 0.1 MHz (Fig. 4b). This result matches well with the calculated DHH condition of Ω_A= 10.44 MHz. Broadening of the DHH polarization transfer dip, compared to that of SHH, may be due to heating of the coplanar waveguide used to deliver microwave signals.

Next, we park the Rabi frequencies at the HH matching conditions and vary the spin-lock (SL) duration. First, without any driving field applied on NV_B, the NV_A SL signal is measured by sweeping the SL duration time as a reference. Under the SHH matching condition, driven by $\Omega_{B,1}$= 7.56 MHz, NV_A SL coherence is drastically lost at a rate of 119 ± 10 kHz, which is extracted from a fit to the data (Fig. 4c). For $\Omega_A \gg \nu_{dip}$, the calculated effective dipolar coupling strength from Eqn. (2) is $\nu_{eff} \approx \nu_{dip}/2 \approx 130$ kHz, which agrees well with our measurement. Under the DHH matching condition, driven by $\Omega_{B,1}$= 9.59 MHz and $\Omega_{B,2}$= 4.13 MHz, NV_A SL coherence is lost with a reduced rate of 73 ± 10 kHz compared to the SHH condition. This result indicates a reduced effective coupling between NV_A and NV_B; the calculated effective coupling strength is $\nu_{eff} \approx 89$ kHz, which is roughly consistent with our measurement. Note that the measured polarization transfer rates are somewhat lower than the calculated values; also polarization return back to NV_A does not happen with full contrast. We suspect such non-ideal behavior is due to imperfect HH matching conditions resulting from coplanar waveguide heating and drift of the external bias magnetic field during the measurements.

E. Simulation of interaction strength homogenization in a spin ensemble

We simulate strongly-coupled NV spin ensemble dynamics for the doubly dressed state, using a semi-classical model. The doubly dressed state scheme induces a homogeneity of spin interaction strengths, which can enhance the fidelity of generating many-spin entangled states [29]. Here, we assume a 50 ppm NV concentration with no other defect spin species present; implying a mean distance between NV spins of ∼5 nm, which is in the strong coupling regime for a Carr-Purcell-Meiboom-Gill (CPMG) pulse enhanced decoherence rate $1/T_2 < 0.2$ MHz [30]. One way to understand the ensemble spin dynamics is to adopt a spin bath spectral density model, parameterized with Δ, the spin to bath coupling, and R_{dd}, the pairwise bath spin-spin coupling [26]. In the simulation, NV ensemble spins are simplified into a collection of two-spin pairs, similar to the approximation applied in a second order cluster correlation expansion (CCE2) calculation [31, 32]. For more detailed discussion on the simulation method, see the supplementary material Appendix D.

We use a central spin model and extract an overall effective dipolar interaction $\Delta^2 = \sum_k \nu_{eff,k}^2$ between the central NV and off-axis NV bath spins [26]. Different lattice configurations are simulated and contribute to a statistical distribution of Δ values. The effect of the doubly dressed state scheme is included by adding driving field terms to the spin pair Hamiltonian. The effective dipolar interaction strength distribution follows a probability density function (PDF); and by assessing the resulting PDF peak position and full width half maximum (FWHM) values, we can estimate the overall spin interaction dynamics. With single transition driving of Rabi frequency $\Omega_1 = 50$ MHz ($|0\rangle \leftrightarrow |+1\rangle$), both the PDF peak and FWHM are reduced by almost half compared to that for the not driven (ND) case (Fig. 5a). This

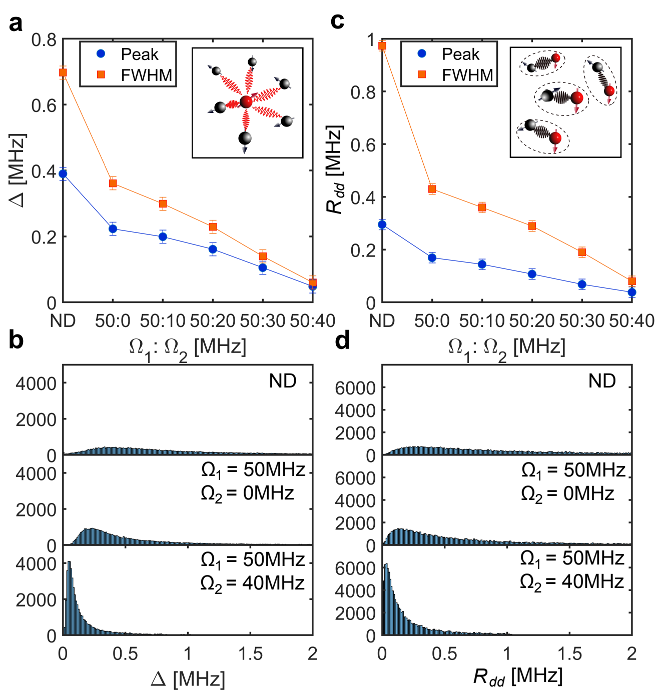

FIG. 5. Semi-classical simulation of effective dipolar couplings for an NV spin ensemble in the doubly dressed state. (a) Using a central spin model(inset), the effective coupling strength Δ between the central NV and the off-axis NV spin bath is calculated for multiple lattice configurations by varying the double transition driving field Rabi frequencies. The resulting Δ probability and distribution displayed are extracted. (b) PDF for Δ when off-axis bath NV spins are not driven (ND); singly driven $\Omega_1 = 50$ MHz, $\Omega_2 = 0$; and doubly driven with $\Omega_1 = 50$ MHz, $\Omega_2 = 40$ MHz. (c) Extracted PDF properties for pairwise flip-flop rates R_{dd} by varying $\Omega_{1,2}$. As shown in the inset figure, among 4 different NV crystalline axis classes, one class (red) is fixed with no driving and 3 other off axis classes (black) are driven. (d) PDF for R_{dd} when pairwise off-axis NV spins are not driven (ND); singly driven with $\Omega_1 = 50$ MHz, $\Omega_2 = 0$; and doubly driven with $\Omega_1 = 50$ MHz, $\Omega_2 = 40$ MHz.

trend continues as an additional second driving field Ω_2 ($|0\rangle \leftrightarrow |-1\rangle$) is introduced, pushing Δ from the strongly coupled to weakly coupled regime. With $\Omega_2 = 40$ MHz, Δ is peaked at 48 ± 10 kHz, compared to the expected effective coupling of 43 kHz deduced from the Eqn. (2) using a bare dipolar coupling of 390 kHz extracted from the ND case (Fig. 5b). Next, we select pairs of off-axis NVs with the strongest coupling over the ensemble of spins and simulate the statistical distribution of pairwise dipole interaction strengths, $\max(\nu_{ij}) = R_{dd}$. Among the four different NV crystalline axis classes, one class is fixed with no driving and the three other off-axis classes are driven. With single transition driving of $\Omega_1 = 50$ MHz, both the PDF peak and FWHM are reduced almost in half (Fig. 5c); and the trend continues as a second driving field Ω_2 is applied. For example, the FWHM for doubly dressed states is 80 ± 10 kHz with $\Omega_1 = 50$ MHz, $\Omega_2 = 40$ MHz; whereas the effective dipolar coupling value from Eqn. (2) is $\nu_{eff} \approx 107$ kHz for an ND FWHM of 973 kHz, implying more uniformity in collective coupling strengths (Fig. 5d). From the simulation results, the doubly dressed state scheme both suppresses interactions between the central NV spin and off-axis NV bath spins and reduces variation of spin-spin coupling strengths, making the ensemble spin system more uniform for coherent manipulation.

III. SUMMARY AND OUTLOOK

To summarize, we demonstrated experimentally the use of dressed-state techniques to control the effective dipolar interaction in a strongly-coupled, solid-state electronic spin-1 system. Using a strongly-coupled pair of nitrogen vacancy (NV) centers in diamond as a toy model, with ν being the bare NV-NV dipolar coupling strength, we induced Rabi driving between different ground spin state sub-levels ($|0\rangle \leftrightarrow |\pm 1\rangle$) and employed a doubly dressed-state to tune the effective coupling strength between $-\nu/2 < \nu_{eff} < +\nu/2$, which was spectroscopically observed via Ramsey measurements. Other pulse schemes [5, 33] to manipulate or suppress effective couplings are comparatively more complicated, with the duration and fidelity of the engineered Hamiltonian typically limited by pulse errors. In contrast, the doubly dressed state scheme provides a robust method to tune the effective coupling dynamics in a qutrit system once the driving strength is larger than the bare dipolar coupling strength ν. For instance, this method could be used to control the order parameter in a disordered spin system to study the transition of non-equilibrium phases [1]. Furthermore, reducing the local distribution of spin couplings could be used to increase fidelity in the generation of collective non-classical states. For example, creating an emergent Greenberger–Horne–Zeilinger (GHZ) state via quantum domino dynamics [34] in an Ising spin chain largely depends on the interaction uniformity [29, 35]. Also, better fidelity generation of a many-spin Schrodinger cat state could be a valuable resource for enhanced quantum sensing or quantum information applications.

ACKNOWLEDGMENTS

This material is based upon work supported by, or in part by, the US Army Research Laboratory and the U.S. Army Research Office under contract/grant numbers W911NF1510548 and W911NF1110400; the NSF Electronics, Photonics, and Magnetic Devices program under Grant No. ECCS-1408075; the NSF Physics of Living Systems program under Grant No. PHY-1504610; and the Integrated NSF Support Promoting Interdisciplinary Research and Education program under Grant No. EAR-1647504. This work was performed in part at the Center for Nanoscale Systems, a member of the National Nanotechnology Coordinated Infrastructure Network, which is supported by the NSF under Grant No. 1541959. J. L was supported by an ILJU Graduate Fellowship and the KIST research program (2E31531). MT is supported by JSPS fellowship (JSPS KAKENHI Grant No. 20J01757). We thank Keigo Arai and Huiliang Zhang for helpful discussions.

---

[1] G. Kucsko, S. Choi, J. Choi, P. C. Maurer, H. Zhou, R. Landig, H. Sumiya, S. Onoda, J. Isoya, F. Jelezko, E. Demler, N. Y. Yao, and M. D. Lukin, Critical thermalization of a disordered dipolar spin system in diamond, Physical Review Letters **121**, 023601 (2018).

[2] S. Choi, J. Choi, R. Landig, G. Kucsko, H. Zhou, J. Isoya, F. Jelezko, S. Onoda, H. Sumiya, V. Khemani, C. Keyserlingk, N. Y. Yao, E. Demler, and M. D. Lukin, Observation of discrete time-crystalline order in a disordered dipolar many-body system, Nature **543**, 221–225 (2017).

[3] C. Zu, F. Machado, B. Ye, S. Choi, B. Kobrin, T. Mittiga, S. Hsieh, P. Bhattacharyya, M. Markham, D. Twitchen, A. Jarmola, D. Budker, C. R. Laumann, J. E. Moore, and N. Y. Yao, Emergent hydrodynamics in a strongly interacting dipolar spin ensemble, Nature **597**, 45 (2021).

[4] A. Cooper, W.-K. C. Sun, J.-C. Jaskula, and P. Cappellaro, Environment-assisted quantum-enhanced sensing with electronic spins in diamond, Physical Review Applied **12**, 044047 (2019).

[5] H. Zhou, J. Choi, S. Choi, R. Landig, A. M. Douglas, J. Isoya, F. Jelezko, S. Onoda, H. Sumiya, P. Cappellaro, H. S. Knowles, H. Park, and M. D. Lukin, Quantum metrology with strongly interacting spin systems, Physical Review X **10**, 031003 (2020).

[6] T. Xie, Z. Zhao, X. Kong, W. Ma, M. Wang, X. Ye, P. Yu, Z. Yang, S. Xu, P. Wang, Y. Wang, F. Shi, and J. Du, Beating the standard quantum limit under ambient conditions with solid-state spins, Science Advances **7**, 32 (2021).

[7] Y. Mindarava, R. Blinder, C. Laube, W. Knolle, B. Abel, C. Jentgens, J. Isoya, J. Scheuer, J. Lang, I. Schwartz, B. Naydenov, and F. Jelezko, Efficient conversion of nitrogen to nitrogen-vacancy centers in diamond particles with high-temperature electron irradiation, Carbon **170**, 182–190 (2020).

[8] J. Choi, H. Zhou, S. Choi, R. Landig, W. Ho, J. Isoya, F. Jelezko, S. Onoda, H. Sumiya, D. A. Abanin, and M. D. Lukin, Probing quantum thermalization of a disordered dipolar spin ensemble with discrete time-crystalline order, Physical Review Letters **122**, 043603 (2019).

[9] J. P. Biersack and L. G. Haggmark, A monte carlo computer program for the transport of energetic ions in amorphous targets, Nuclear Instruments and Methods **174**, 257 (1980).

[10] J. Meijer, B. Burchard, M. Domhan, C. Wittmann, T. Gaebel, I. Popa, F. Jelezko, and J. Wrachtrup, Generation of single colour centres by focused nitrogen implantation, Applied Physics Letters **87**, 261909 (2005).

[11] T.-Y. Hwang, J. Lee, S.-W. Jeon, Y.-S. Kim, Y.-W. Cho, H.-T. Lim, S. Moon, S.-W. Han, Y.-H. Choa, and H. Jung, Sub-10 nm precision engineering of solid-state defects via nanoscale aperture array mask, Nano Letters **22**, 1672 (2022).

[12] I. Jakobi, S. A. Momenzadeh, F. F. D. Oliveira, J. Michl, F. Ziem, M. Schreck, P. Neumann, A. Denisenko, and J. Wrachtrup, Efficient creation of dipolar coupled nitrogen-vacancy spin qubits in diamond, Journal of Physics: Conference Series **752**, 012001 (2016).

[13] F. de Oliveira, D. Antonov, Y. Wang, S. A. M. P. Neumann, T. Häußermann, A. Pasquarelli, A. Denisenko, and J. Wrachtrup, Tailoring spin defects in diamond by lattice charging, Nature Communications **8**, 15409 (2017).

[14] A. M. Edmonds, U. F. S. D'Haenens-Johansson, R. J. Cruddace, M. E. Newton, K.-M. C. Fu, C. Santori, R. G. Beausoleil, D. J. Twitchen, and M. L. Markham, Production of oriented nitrogen-vacancy color centers in synthetic diamond, Phyiscal Review B **86**, 035201 (2012).

[15] A. M. Rey, L. Jiang, M. Fleischhauer, E. Demler, and M. D. Lukin, Many-body protected entanglement generation in interacting spin systems, Physical Review A **77**, 052305 (2008).

[16] A. Gali, Theory of the neutral nitrogen-vacancy center in diamond and its application to the realization of a qubit, Physical Review B **79**, 235210 (2009).

[17] T. Gaebel, M. Domhan, I. Popa, C. Wittmann, P. Neumann, F. Jelezko, J. R. Rabeau, N. Stavrias, A. D. Greentree, S. Prawer, J. Meijer, J. Twamley, P. R. Hemmer, and J. Wrachtrup, Room-temperature coherent coupling of single spins in diamond, Nature Physics **2**, 408 (2006).

[18] F. Dolde, I. Jakobi, B. Naydenov, N. Zhao, S. Pezzagna, C. Trautmann, J. Meijer, P. Neumann, F. Jelezko, and J. Wrachtrup, Room-temperature entanglement between single defect spins in diamond, Nature Physics **9**, 139 (2013).

[19] A. Abragam, The principles of nuclear magnetism (Clarendon Press, 1961).

[20] J. N. Mundy, Solid state : Nuclear methods (Academic Press, 1983) Chap. 6.2.1.1.

[21] J. Li, M. Silveri, K. Kumar, J.-M. Pirkkalainen, A. Vepsalainen, W. Chien, J. Tuorila, M. Sillanpaa, P. Hakonen, E. Thuneberg, and G. Paraoanu, Motional averaging in a superconducting qubit, Nature Communications **4**, 1420 (2013).

[22] G. de Lange, T. van der Sar, M. Blok, Z. Wang, V. Dobrovitski, and R. Hanson, Controlling the quantum dynamics of a mesoscopic spin bath in diamond, Scientific Reports **2**, 382 (2012).

[23] E. Bauch, C. A. Hart, J. M. Schloss, M. J. Turner, J. F. Barry, P. Kehayias, and R. L. Walsworth, Ultralong dephasing times in solid-state spin ensembles via quantum control, Physical Review X **8**, 031025 (2018).

[24] C. Senko, P. Richerme, J. Smith, A. Lee, I. Cohen, A. Retzker, and C. Monroe, Realization of a quantum integer-spin chain with controllable interactions, Physical Review X **5**, 021026 (2015).

[25] T. Yamamoto, C. Müller, L. P. McGuinness, T. Teraji, B. Naydenov, S. Onoda, T. Ohshima, J. Wrachtrup, F. Jelezko, and J. Isoya, Strongly coupled diamond spin

qubits by molecular nitrogen implantation, Physical Review B **88**, 201201(R) (2013).

[26] E. Bauch, S. Singh, J. Lee, C. A. Hart, J. M. Schloss, M. J. Turner, J. F. Barry, L. M. Pham, N. Bar-Gill, S. F. Yelin, and R. L. Walsworth, Decoherence of ensembles of nitrogen-vacancy centers in diamond, Physical Review B **102**, 134210 (2020).

[27] C. Belthangady, N. Bar-Gill, , L. M. Pham, K. Arai, D. L. Sage, P. Cappellaro, and R. L. Walsworth, Dressed-state resonant coupling between bright and dark spins in diamond, Physical Review Letters **110**, 157601 (2013).

[28] S. R. Hartmann and E. L. Hahn, Nuclear double resonance in the rotating frame, Physical Review **128**, 2042 (1962).

[29] A. Yoshinaga, M. Tatsuta, and Y. Matsuzaki, Entanglement-enhanced sensing using a chain of qubits with always-on nearest-neighbor interactions, Physical Review A **103**, 062602 (2021).

[30] N. Bar-Gill, L. Pham, C. Belthangady, D. L. Sage, P. Cappellaro, J. Maze, M. Lukin, A. Yacoby, and R. Walsworth, Suppression of spin-bath dynamics for improved coherence of multi-spin-qubit systems, Nature Communications **3**, 858 (2012).

[31] W. M. Witzel and S. D. Sarma, Quantum theory for electron spin decoherence induced by nuclear spin dynamics in semiconductor quantum computer architectures: Spectral diffusion of localized electron spins in the nuclear solid-state environment, Physical Review B **74**, 035322 (2006).

[32] W. Yang and R.-B. Liu, Quantum many-body theory of qubit decoherence in a finite-size spin bath. ii. ensemble dynamics, Physical Review B **79**, 115320 (2009).

[33] S. Choi, N. Y. Yao, and M. D. Lukin, Dynamical engineering of interactions in qudit ensembles, Physical Review Letters **119**, 183603 (2017).

[34] J.-S. Lee and A. K. Khitrin, Stimulated wave of polarization in a one-dimensional ising chain, Physical Review A **71**, 062338 (2005).

[35] J. Zhang, F. M. Cucchietti, C. M. Chandrashekar, M. Laforest, C. A. Ryan, M. Ditty, A. Hubbard, J. K. Gamble, and R. Laflamme, Direct observation of quantum criticality in ising spin chains, Physical Review A **79**, 012305 (2009).